to the deuterons of free bpy and two more signals at 7.7 and 10.1 ppm assigned to a diamagnetic complex.

The $^2$H NMR spectrum of Cr(bpy-$6,6'$-$d_2$)$_3$(PF$_6$)$_3$ in acetone (Figure 2) yields only one signal at $-97$ ppm, indicating equivalence of all six deuterons of the three bpy ligands and implying the expected $D_3$ symmetry of the complex.

In DMF the cyclic voltammogram of the dissolved Mo-(bpy)$_3$(PF$_6$)$_3$ exhibits two reversible reduction waves at $-0.58$ and $-1.05$ V and one irreversible oxidation wave at 1.00 V (Table I).

The spin-only magnetic moment expected for an octahedral d$^3$ complex is $\mu_{eff} = 3.87$ $\mu_B$.[16]    After one recrystallization Mo-(bpy)$_3$(PF$_6$)$_3$ has a magnetic moment of 3.54 $\mu_B$. Two more recrystallizations yield a product that has a correct C,H,N analysis but a strongly diminished magnetic moment (0.1 $\mu_B$).

## Discussion

There is no doubt that for the solid state all analytical data (IR, elemental analysis) agree with a formulation of Mo(bpy)$_3$(PF$_6$)$_3$ as a salt of the octahedral complex Mo(bpy)$_3^{3+}$. The spectroscopic data of Mo(bpy)$_3$(PF$_6$)$_3$ and Mo(bpy-$6,6'$-$d_2$)$_3$(PF$_6$)$_3$ in acetone, in DMF, or in MeOH are inconsistent with the assumption of an octahedral $D_3$ tris-chelate complex.

The solution behavior, i.e. reduction of the $D_3$ symmetry as observed by $^2$H NMR, could be due to the following reasons: (a) oxidation, (b) coordination number greater than 6, (c) polymerization, and (d) loss of one bpy.

The resonances at $-69$ and $-94$ ppm for the deuterons bound to a paramagnetic species are typical for three unpaired electrons, therefore excluding reason a.

A coordination number greater than 6 would not explain the signal of the deuterons bound to free bpy. A polymerization with one or two bridging bpy's will give more than two resonances of equal intensities in the paramagnetic region.

The substitution of one bpy by the solvent results in a bis-chelate complex: Mo$^{III}$(bpy)$_2$(solvent)$_2^{3+}$. In the case where the two solvent molecules are in cis positions, the six deuterons bound to the paramagnetic species produce two resonances of equal intensity. The deuterons belonging to the liberated bpy show one signal at 8 ppm.

The $^2$H NMR spectrum is entirely in agreement with this interpretation. This result shows that in solution the Mo(bpy)$_3^{3+}$ is thermodynamically unstable and dissociates rapidly into Mo-(bpy)$_2$(solvent)$_2^{3+}$ and bpy.

The resonances at 7.7 and 10.1 ppm and the decreased magnetic moments of products, which were recrystallized several times, could be due to the formation of polymers, stabilized by Mo–Mo bonds. Attempts to prepare salts of Mo(bpy)$_2$((CH$_3$)$_2$CO)$_2^{3+}$ failed, due to the formation of polymeric products that cannot easily be characterized. The signals in the $^2$H NMR spectra at $-69$ and $-94$ ppm disappear after several days completely even if oxygen is strictly excluded. Several signals in the "diamagnetic" region indicate the presence of more than one species.

It would be interesting to compare the $^2$H NMR spectrum of Mo(bpy-$6,6'$-$d_2$)$_2$(solvent)$_2^{3+}$ with the $^2$H NMR spectrum of Cr(bpy-$6,6'$-$d_2$)$_2$(solvent)$_2^{3+}$, but unfortunately no resonance was observed for the latter complex between +20 and $-200$ ppm.

The hypothesis of rapid dissociation of one bpy ligand deduced from $^2$H NMR data is corroborated by the redox behavior (Table I). The cyclic voltammogram of "Mo(bpy)$_3^{3+}$" in DMF solution is very similar to that of Mo(bpy)$_2$Cl$_2^+$ but different from the second and third oxidation waves of Mo(bpy)$_3$. The third oxidation wave of neutral Mo(bpy)$_3$, on the other hand, is irreversible, indicating the instability of Mo(bpy)$_3^{3+}$.

## Conclusion

The difficulties in preparing Mo(bpy)$_3^{3+}$, mentioned in the literature[8,18,19] and reiterated in our laboratory, can now be explained as follows:

(16) Figgis, B. N.; Lewis, J.; Mabbs, F. E. *J. Chem. Soc.* **1961**, 3138.
(17) Dubois, D. W.; Iwamoto, R. T.; Kleinberg, J. *Inorg. Chem.* **1970**, *9*, 968.
(18) Marzili, P.; Buckingham, D. A. *Aust. J. Chem.* **1966**, *19*, 2259.
(19) Furlani, C.; Piovesana, O. *Mol. Phys.* **1965**, *9*, 341.

Contrary to the widespread belief that 4d$^3$ second-row transition elements form complexes more inert than first-row 3d$^3$ elements, Mo(III) seems to be much more substitutionally labile than Cr(III), at least with bpy ligands. Moreover, Mo(bpy)$_3^{3+}$ is thermodynamically unstable toward dissociation of one bpy ligand in most common solvents. Formation of the tris complex in the solid state is due to the insolubility of Mo(bpy)$_3$(PF$_6$)$_3$. Two alternative pathways for the rapid dissociation reaction can be envisaged: (a) accessibility of an associative pathway for the substitution reaction and (b) catalytic amounts of complexes having higher oxidation states of Mo initiating the substitution of a bpy ligand.

Contribution from the Laboratoire de Spectrochimie des Elements de Transition et CNRS, UA 420, and Laboratoire de Chimie Théorique et CNRS, UA 506, Université de Paris-Sud, 91405 Orsay, France

## On the Electronic Structure of MPS$_3$ Phases

Helène Mercier,[†§] Yves Mathey,[*†‖] and Enric Canadell[*‡]

Because of their topochemical,[1,2] electrochemical,[3] optical,[4–6] and magnetic[4,7–9] properties, two-dimensional materials of the MPS$_3$ family (Figure 1) have been the subject of intense investigation during the past decade. As a result, there is now a wealth of experimental data concerning these remarkable systems. Nevertheless, the rationalization of some of these data has led to a series of very puzzling questions. This was in part due to the absence of detailed band structures for these materials.

Recently Whangbo, Brec, Ouvrard, and Rouxel[10] reported an extended Hückel tight-binding analysis of the electronic structure of FePS$_3$. They were able to show that the acceptor levels under alkali-metal intercalation are the partially filled 3d orbitals. Later, Brec, Whangbo, et al.[11] interpreted some unusual Mössbauer phenomena in Li$_x$FePS$_3$ using similar computations. Since revised structural data on many of these phases have recently appeared,[12] we felt it useful to look again at their electronic structure. Therefore, we have carried out extended Hückel tight-binding calculations on a series of MPS$_3$ systems (M = Mn, Fe, Co, Ni, Cd) using parameters and exponents given in the Appendix.

The computed densities of states for all these phases have a number of common features schematically shown in **1**. A sizable



**1**
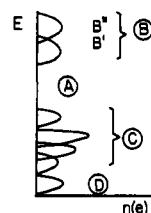
gap (A) separates the predominantly metal region (C) from what would be the lowest empty levels region for d$^{10}$ cases (B). B contains two contributions, the lowest one (B') being predominantly made of the s and p levels of the metal. The P–P (and

†Laboratoire de Spectrochimie des Elements de Transition.
‡Laboratoire de Chimie Théorique.
§Present address: Laboratoire des Acides Mineraux, UA CNRS 79, Université de Montpellier 2, 34060, Montpellier, France.
‖Present address: Département de Physique, Faculté des Sciences de Luminy, Case 901, 13288 Marseille, France.
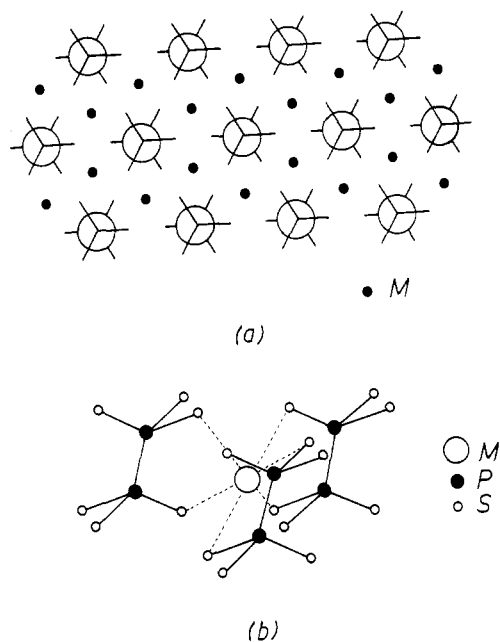
(a)



○ M
● P
○ S

(b)

**Figure 1.** Structure of a layer in $MPS_3$ phases: (a) top view; (b) local structure.
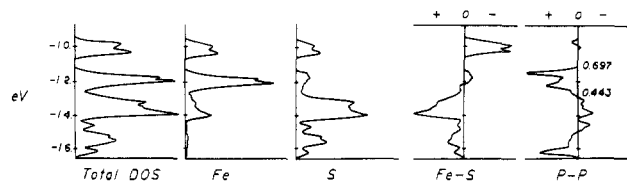


**Figure 2.** Total density of states, Fe and S projected densities of states, and Fe–S and P–P COOP curves for $FePS_3$. The numerical values in the P–P COOP curve are the integrated overlap populations assuming double occupation of the levels.

P–S) antibonding levels appear only at higher energies (B''). We emphasize this fact because in several instances it has been suggested that the $\sigma^*$ P–P levels are the acceptor sites for $CdPS_3$.[1,13]

Of more interest to us is region C, which we will analyze in detail for the specific case of $FePS_3$. Shown in Figure 2 are the total density of states (DOS) as well as the projections of the Fe and S contributions and the COOP (crystal orbital overlap population) curves[14] for Fe–S and P–P. The projection of the Fe

**Table I.** Experimental Values[12] for the P–P Distance in Different $MPS_3$ Phases

| $M^{II}$ | config | $d_{P-P}$, Å | $M^{II}$ | config | $d_{P-P}$, Å |
|---|---|---|---|---|---|
| Mn | $t_{2g}^3 e_g^{*2}$ | 2.187 | Ni | $t_{2g}^6 e_g^{*2}$ | 2.148 |
| Fe | $t_{2g}^4 e_g^{*2}$ | 2.174 | Zn | $t_{2g}^6 e_g^{*4}$ | 2.188 |
| Co | $t_{2g}^5 e_g^{*2}$ | 2.165 | | | |

orbitals shows three contributions: a strong peak centered at $-11.9$ eV (near the value for the Fe 3d $H_{ii}$ parameter) and two smaller peaks at $-13.8$ and $-10.2$ eV. Whereas there are important contributions of sulfur orbitals at $-13.8$ and $-10.2$ eV, that at $-11.9$ eV is noticeably smaller. This immediately suggests that the peak at $-10.2$ eV in the total DOS contains the Fe–S $e_g^*$ levels, the peak at $-11.9$ eV contains the Fe $t_{2g}$ orbitals, and the lowest part of the peak at $-13.8$ eV contains the Fe–S $e_g$ levels.[15] This is confirmed by the Fe–S COOP curve of Figure 2. In fact, the $e_g$ levels partially overlap with a strong peak that contains the sulfur lone pairs, and this is why we have disclosed this peak into two contributions in the schematic DOS shown in 1. The P–S bonding levels are found just below (peak D in 1).

Perhaps more surprising is the P–P COOP curve (Figure 2). It can be seen that there is a peak (actually split into two) coincident in energy with the $t_{2g}$ metal contribution. *This peak accounts for somewhat more than one-third of the P–P overlap population calculated for a $d^{10}$ metal case.* The complete P–P COOP curve presents two additional positive contributions at lower energies where the P–S contributions are also found.

Since these results are common to the different $MPS_3$ phases studied, three remarks can be made at this point. First, the $e_g^*$ peak is found nearly 2 eV (or more) higher than the $t_{2g}$ one and is made of *both* metal and sulfur orbitals. This clearly shows that the metal–sulfur interaction, although not as strong as in the directly bonded case, is by no means negligible as it was assumed in the weak interaction model.[16,17] Second, the overlap populations calculated for the P–P and P–S bonds are very similar (0.71 and 0.74, respectively, for a $d^{10}$ system). This invalidates the second assumption of the weak interaction model, i.e., that the P–P bond is very weak. Third, the fact that the P–P bonding levels are split into three peaks that are located in regions containing the *strong* M $t_{2g}$ and bonding P–S contributions explains why Piacentini et al.[17,18] did not observe a bonding P–P band in the XPS spectra of $FePS_3$ and $NiPS_3$.

Why about one-third of the P–P bonding levels appear in the M $t_{2g}$ region of the DOS is easy to see. The pyramidalization angle of the $PS_3$ group is such that there is a good overlap between the $p_z$ orbital of phosphorus and the mainly $p_z$ sulfur lone pairs. As a result, the HOMO of $P_2S_6^{4-}$ acquires a sizable P–P bonding contribution (see 2). If this HOMO can interact with the metal



2
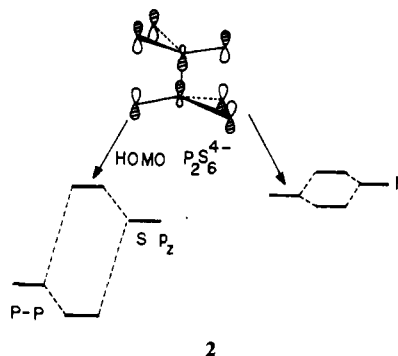
$t_{2g}$ orbitals, part of the P–P bonding will be found in the M $t_{2g}$

(1) Johnson, J. W. In *Intercalation Chemistry*; Whittingham, M. S., Jacobson, A. J., Eds.; Academic: New York, 1982; p 267.
(2) Clement, R.; Garnier O.; Jegoudez, J. *Inorg. Chem.* **1986**, *25*, 1404. Clement, R. *J. Chem. Soc., Chem. Commun.* **1980**, 647.
(3) Brec, R.; Ouvrard, G.; Louisy, A.; Rouxel, J.; Le Mehauté, A. *Solid State Ionics* **1982**, *6*, 185.
(4) Brec, R.; Schleich, D. M.; Ouvrard, G.; Louisy, A.; Rouxel, J. *Inorg. Chem.* **1979**, *18*, 1814.
(5) Grasso, V.; Santangelo, S.; Piacentini, M. *Solid State Ionics* **1986**, *20*, 9.
(6) Mercier, H.; Mathey, Y. *Nouv. J. Chim.* **1986**, *10*, 473.
(7) Le Flem, G.; Brec. R.; Ouvrard, G.; Louisy A.; Segransan, P. *J. Phys Chem. Solids* **1982**, *43*, 455. Ouvrard, G.; Brec, R.; Rouxel, J., *C. R. Seances Acad. Sci.* **1982**, *294*, 971. Taylor, B. E.; Steger, J.; Wold, A. *J. Solid State Chem.* **1973**, *7*, 461.
(8) Clement, R.; Girerd, J. J.; Morgenstern-Badarau, I. *Inorg. Chem.* **1980**, *19*, 2850.
(9) Clement, R.; Garnier, O.; Mathey, Y. *Nouv. J. Chim.* **1982**, *6*, 13.
(10) Whangbo, M.-H.; Brec, R.; Ouvrard, G.; Rouxel, J. *Inorg. Chem.* **1985**, *24*, 2459.
(11) Fatseas, G. A.; Evain, M.; Ouvrard, F.; Brec. R.; Whangbo, M.-H. *Phys. Rev. B.*, in press.
(12) (a) Ouvrard G.; Brec, R.; Rouxel, J. *Mater. Res. Bull.* **1985**, *20*, 1181. (b) Prouzet, E.; Ouvrard, G.; Brec. R. *Mater. Res. Bull.* **1985**, *21*, 195.
(13) Bal, B.; Ganguly, G.; Battacharya, M. *Physica B+C (Amsterdam)* **1985**, *133B+C*, 64.
(14) Such curves were introduced in: Hughbanks, T.; Hoffmann, R. *J. Am. Chem. Soc.* **1983**, *105*, 3528.

(15) The $t_{2g}$ and $e_g$ labels are only approximate and are used in a purely descriptive manner since the local environment of the metal atoms is a distorted octahedron.
(16) Khumalo, F. S.; Hughes, H. P. *Phys. Rev. B* **1981**, *23*, 5375.
(17) Piacentini, M.; Khumalo, F. S.; Olson, C. G.; Anderegg, J. W.; Lynch, D. W. *Chem. Phys.* **1982**, *65*, 289.
(18) Piacentini, M.; Grasso, M.; Santangelo, S.; Fanfoni, M.; Modesti, S.; Savoia, A. *Nuovo Cimento D* **1984**, *4*, 444.
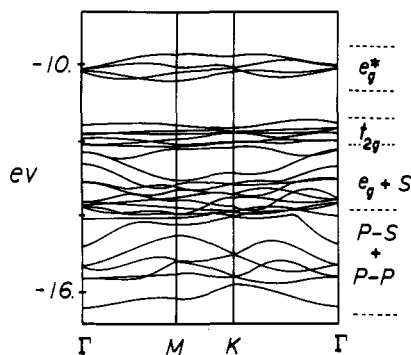
**Figure 3.** Band structure for $FePS_3$. $\Gamma$, K, and M refer to the points (0, 0), $(^1/_3, ^1/_3)$, and $(^1/_2, 0)$ of the 2-D hexagonal Brillouin zone. The main character of the bands is indicated on the right.

peak of the DOS. Since the octahedral environment of each metal atom is a distorted one and the actual symmetry is only $D_{3d}$, this interaction is possible. Indeed, a detailed analysis of the band structures shows that this interaction is effectively at work. Although this interaction is per force weak, it is sufficient to split the peak in the P–P COOP curve into two subpeaks.

The above discussion not only allows a *chemical description* of the DOS but points out an electron-dependent structural trend. Since the metal atoms are in a high-spin configuration,[7] it is clear that the $t_{2g}$ peak is progressively filled from $MnPS_3$ to $NiPS_3$. Therefore, due to the participation of $\sigma$ P–P in this peak, *there is an electronic effect influencing the P–P bond length* in addition to the ion size. The P–P distance should decrease from $MnPS_3$ to $NiPS_3$, and indeed this is what has been found by Ouvrard, Brec, and Rouxel[12] (Table I). Once the $t_{2g}$ levels are filled (i.e. $NiPS_3$), the electronic effect is no longer operative and only the ion size effect remains.[19] The P–P distance should increase again, as it does.[12b] It is difficult at this point to elucidate whether the electronic or the ion size effect plays the dominant role. In this respect it would be interesting to study the structural consequences of the step-by-step electrochemical reduction of systems with incomplete $t_{2g}$ levels, such as $MnPS_3$ and $FePS_3$.

Additional information can be gained from consideration of the detailed band structures. That corresponding to $FePS_3$ is reported in Figure 3.[20] The $e_g^*$, $t_{2g}$, and $e_g$ bands can be easily recognized at the top and middle of the figure. As it is the case for the other $MPS_3$ phases studied, the dispersion of the $t_{2g}$ and $e_g^*$ bands is low so that a localized state is favored, explaining the high resistivity values.[14] Nevertheless, as pointed out in our discussion of the $t_{2g}$ peak or from the approximately 0.5-eV ·dispersion of the $e_g^*$ bands, we have to conclude that the different $MX_6$ octahedra are *weakly coupled* as long as the $t_{2g}$ and $e_g^*$ bands are concerned. This means that the magnetic behavior of these phases should be modified by intercalation. Indeed, very strong changes have been reported in the case of $MnPS_3$, $FePS_3$, and $NiPS_3$ under cobaltocinium intercalation.[8,9] It is then quite puzzling that such changes have not been reported for $FePS_3$, $FePSe_3$, and $MnPSe_3$ under lithium intercalation.[4]

Whangbo et al.[10] have proposed that the more intense optical absorption is associated with an $e_g \rightarrow e_g^*$ excitation. Except for the case of $NiPS_3$, the $e_g$ and $e_g^*$ bands are well separated and relatively flat. A molecular model is then valid to interpret the values of the observed absorption-edge energies. Since the $e_g$ bands are more concentrated on the chalcogen and the $e_g^*$ ones more on the metal, the edge energy should decrease when the electronegativity of the metal increases or when the chalcogen becomes less electronegative. This agrees with the reported data[4] except for the case of $NiPS_3$. When the metal electronegativity increases,

**Table II.** Exponents and Parameters Used in the Calculations

|  |  | $\zeta_\mu$ | $\zeta_\mu'$ | $H_{\mu\mu}$, eV |
|---|---|---|---|---|
| Mn | 4s | 1.8 |  | −8.0 |
|  | 4p | 1.8 |  | −5.0 |
|  | 3d | 5.15 (0.5311)[a] | 1.9 (0.6479)[a] | −11.6 |
| Fe[10] | 4s | 1.9 |  | −8.4 |
|  | 4p | 1.9 |  | −5.0 |
|  | 3d | 5.35 (0.5505) | 2.0 (0.6260) | −12.2 |
| Co | 4s | 2.0 |  | −9.2 |
|  | 4p | 2.0 |  | −5.3 |
|  | 3d | 5.55 (0.5674) | 2.1 (0.6059) | −13.0 |
| Ni | 4s | 2.1 |  | −10.95 |
|  | 4p | 2.1 |  | −6.27 |
|  | 3d | 5.75 (0.5862) | 2.2 (0.5846) | −13.7 |
| Cd | 5s | 2.3 |  | −12.5 |
|  | 5p | 2.1 |  | −6.6 |
|  | 4d | 6.38 (0.6404) | 2.81 (0.5203) | −14.6 |
| P | 3s | 1.88 |  | −20.2 |
|  | 3p | 1.63 |  | −12.5 |
| S | 3s | 2.12 |  | −20.1 |
|  | 3p | 1.83 |  | −13.3 |

[a] Contraction coefficients used in the double-$\zeta$ expansion.

its d levels can eventually become lower than the sulfur lone pairs, and in that case, the relative weight of the M and X orbitals on the $e_g$ and $e_g^*$ levels should be reversed. Indeed, this is what is found in our calculations for $NiPS_3$. If real, this fact should have two effects on the optical spectra of these phases. First, going from $MnPS_3$ to $NiPS_3$, the absorption-edge energy should initially decrease and then increase. Second, the edge energy should increase when going from $MPS_3$ to $MPSe_3$ for M = Ni instead of decreasing when M = Mn. The first point is supported by our recent reexamination of the $NiPS_3$ optical spectrum.[6] The location of the absorption edge was there unambiguously given in the UV energy region, i.e. far higher in energy than the one previously proposed.[4] Unfortunately, there are still no experimental results to check the second point. Another consequence of the low energy of the Ni d levels is that the $e_g$, $t_{2g}$, and sulfur lone pair bands of $NiPS_3$ overlap in a much more intricate manner than in the band structures of $MnPS_3$ or $FePS_3$. It then appears that some of the sulfur lone pair bands—now among the highest of the C block (see **1**)—acquire metal $e_g$ character. This can lead to supplementary low-energy transitions in the optical spectrum of $NiPS_3$, which should be taken into account.

Although we are still far from a complete understanding of the chemical and physical behavior of the $MPS_3$ phases, we believe that the present results support the idea that the extended Hückel model, as first proposed by Whangbo, Brec, Ouvrard, and Rouxel,[10] provides a much more realistic picture than the weak-interaction model.[16,17] Further work to extend its scope is now in progress.

**Appendix**

The calculations are of the extended Hückel type[21] with exponents and parameters given in Table II. The modified Wolfsberg–Helmholz formula[22] was used. A set of 36K points within the irreducible wedge of the Brillouin zone was used. In all calculations the $P_2S_6$ group was held constant. P–P and P–S distances of 2.19 and 2.03 Å and a P–P–S angle of 104° were used. The metal–sulfur distances were taken from ref 12.

(19) It should be pointed that from Ni to Zn the $e_g^*$ levels are being filled. Although the primary consequence of this should be an increase of the M–S distance, the P–P–S angle and P–P distance could also slightly increase.

(20) Detailed band structures for the other systems studied can be obtained from the authors. Mercier, H. Ph.D. Thesis, Orsay, 1985.

(21) Whangbo, M.-H.; Hoffmann, R. *J. Am Chem. Soc.* **1978**, *100*, 6093. Hoffmann, R. *J. Chem. Phys.* **1963**, *39*, 1397.

(22) Ammeter, J.; Bürgi, H.-B.; Thibeault, J.; Hoffmann, R. *J. Am. Chem. Soc.* **1978**, *100*, 3686.